Available online at www.sciencedirect.com

SciVerse ScienceDirect

Ceramics International 38 (2012) 5113–5121

CERAMICS INTERNATIONAL

www.elsevier.com/locate/ceramint

Effect of physical vapor deposited Al_2O_3 film on TGO growth in YSZ/CoNiCrAlY coatings

Yanjun Li [a], Youtao Xie [a], Liping huang [a], Xuanyong Liu [b], Xuebin Zheng [a,*]

[a] Key Laboratory of Inorganic Coating Materials, Shanghai Institute of Ceramics, Chinese Academy of Sciences, 1295 Dingxi Road, Shanghai, 200050, China
[b] Biomaterials and Tissue Engineering Research Center, Shanghai Institute of Ceramics, Chinese Academy of Sciences, 1295 Dingxi Road, Shanghai, 200050, China

Received 11 January 2012; received in revised form 2 March 2012; accepted 2 March 2012
Available online 13 March 2012

Abstract

Thermal barrier coatings (TBCs) comprising of yttria stabilized zirconia (YSZ) ceramic top coat and CoNiCrAlY metallic bond coat have been widely used in gas turbines. However, the developed oxides layer in the interface of the top and bond coats during thermal exposure of the TBCs always results in the destruction of the system. In order to restrain the growth of oxides layer and improve the thermal shock resistance of TBCs, a thin Al_2O_3 film was pre-deposited on CoNiCrAlY bond coat by physical vapor deposition (PVD) technology. After thermal exposure, morphologies and phase compositions of the thermal growth oxides (TGO) layer in the conventional and pre-deposited Al_2O_3 film TBCs were examined by scanning electron microscopy (SEM) equipped with energy dispersive spectrometer (EDS). The residual stresses in the coatings were analyzed using micro-Raman spectroscopy (LabRam-1B). It was found that TGO layer formed in the conventional TBCs was mainly composed of Al_2O_3, $(Cr,Al)_2O_3$ + $(Co,Ni)(Cr,Al)_2O_4$ + NiO (CSN), and $(Cr,Al)_2O_3$ + $(Co,Ni)(Cr,Al)_2O_4$ (CS), while in the treated TBCs, the formed TGO layer appeared more uniform and compact. The CSN and CS clusters, which are normally considered as a weakness for TBCs, were greatly limited. The residual stresses in the TBCs after thermal shock were also reduced by the deposition of Al_2O_3 film.

Keywords: C. Thermal shock resistance; Al_2O_3 film; Residual stress; Thermal barrier coatings

1. Introduction

Thermal barrier coatings (TBCs) are widely used as protective coatings on hot section components in advanced gas turbine engines to withstand increased inlet temperatures and thus improve engine performance [1,2]. A typical TBC system includes MCrAlY(M = Co and/or Ni) bond coat as oxidation resistant layer and yttria stabilized zirconia (YSZ) as thermal insulation top coat [3,4]. The top coat can reduce the temperature of underlying superalloy in relation to the gas path temperature owing to its low thermal conductivity, while the bond coat enhances the adhesion of the top ceramic layer to the metallic substrate and also provides oxidation and corrosion protection to the substrate [5,6].

When exposed to high temperatures, bond coat can be oxidized resulting in the formation of a thermally grown oxide (TGO) layer at the top coat/bond coat interface. The TGO layer predominantly comprised of Al_2O_3 can provide protection of the underlying substrate against further high-temperature corrosion. However, upon cooling of the component from high temperature, the thermal-mismatch strains develop within the TGO layer [7]. The elastic energy associated with these strains is the main driving force for failure of the coating system. The strain energy normally increases with the thickness of TGO layer [8]. With the thickening of the TGO layer, internal stress increases and finally leads to the spallation failure of TBCs [3,5,13]. Hence, failures of TBCs are often correlated with a critical TGO thickness [9–11]. Recent researches show that failure of some TBC systems occurred when the TGO layer attained to a critical thickness in the range of 3–10 μm [8,12].

Besides the thickness of TGO layers, chemical compositions of TGO layer are also crucial for the failure of TBCs. The oxide scales in TGO layers are not pure Al_2O_3, but also contain some other oxides, such as NiO, Cr_2O_3 and spinel. Alumina exhibits better anti-corrosion properties than other oxides at high

* Corresponding author. Fax: +86 021 52414104.
E-mail address: xbzheng@mail.sic.ac.cn (X. Zheng).

0272-8842/$36.00
doi:10.1016/j.ceramint.2012.03.014

temperature because of its dense microstructure, good adherence and low oxygen diffusivity [14]. Meanwhile, extra stresses could be introduced by the mixture oxides in the top coat/TGO interface. It is therefore crucial to induce the preferential oxidation of Al over other elements to form the more protective and adherent Al_2O_3 component in TGO layer. One choice to enhance the oxidation of Al is to elevate the Al content in the bond coat. However, the increase of Al in the bond coat would reduce the toughness of the coating and decrease its fatigue resistance.

Al_2O_3 is an oxygen barrier material and has been studied as an additive in YSZ/MCrAlY TBC systems. It was reported [3,15,16] that the addition of Al_2O_3 into YSZ could improve the sintering resistance, reduce the thermal conductivity of the YSZ coating, and mitigate the thermal expansion mismatch between bond coat and top coat. Kobayashi et al. [17] deposited a dense Al_2O_3 top layer on YSZ coating, and found the presence of Al_2O_3 film reduced the infiltration of molten salt and resulted in the improved resistance of TBCs against hot corrosion. It is reasonable to deduce that a thin, dense Al_2O_3 film between bond coat and top coat could retard the oxygen penetration in thermal environment, restrain the growth of TGO layer and control the chemical compositions of TGO layer. One of appropriate approaches to obtain such an Al_2O_3 film is physical vapor deposition (PVD). However, few researches were found to focus on the effects of a pre-deposited Al_2O_3 film on TGO layer growth in an YSZ/CoNiCrAlY TBC system.

In this study, a thin Al_2O_3 film was deposited between the CoNiCrAlY bond coat and YSZ top layer. The growth of TGO layer during thermal cyclic processes was monitored and the crack propagations in the TBC system were analyzed.

2. Experimental

Commercially available CoNiCrAlY powder (Metco 995, Sulzer Metco, Switzerland) with median size at 30 μm was applied to prepare bond coat (BC) on nickel-based superalloy (625, Yongfeng, China) with size of 2 × 10 × 20 mm by a vacuum plasma spray (VPS) system (F4-VB, Sulzer Metco, Switzerland). The coatings were deposited under modified deposition parameters as shown in Table 1. The thickness of the bond coat was about 150 μm. A thin Al_2O_3 film was deposited by hollow cathode PVD (PIIIS-700, Shanghai Institute of Ceramics, China) under the parameters tabulated in Table 2. ZrO_2–8 wt.%Y_2O_3 (YSZ) top coat (TC) were subsequently prepared with an air plasma spray (APS) system (F4-MB, Sulzer Metco, Switzerland) using commercial YSZ powder (Metco 204NS, Suler Metco, Switzerland). A similar TBC system without PVD Al_2O_3 film was prepared as comparison.

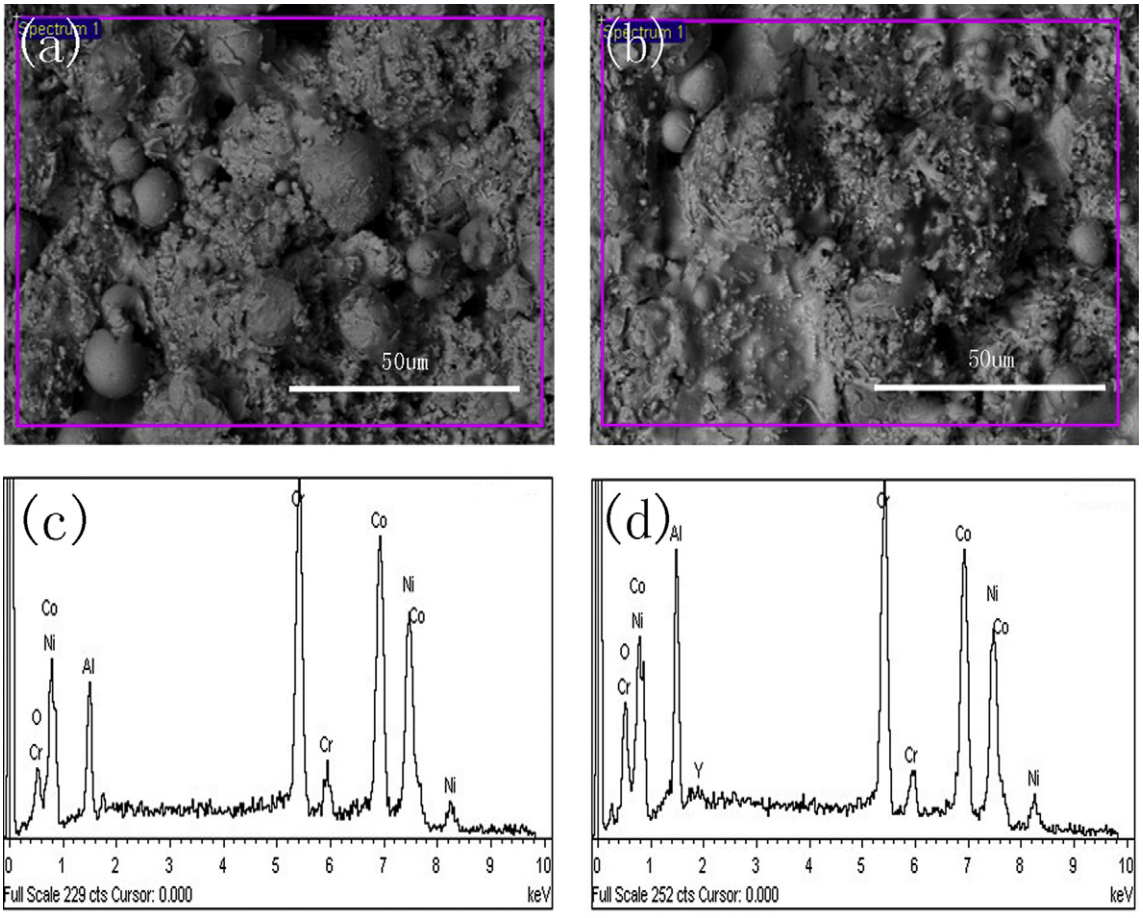

Fig. 1. SEM micrographs and EDS spectra of the CoNiCrAlY bond coat: (a) surface morphology without PVD Al_2O_3 film; (b) surface morphology with PVD Al_2O_3 film; (c) EDS of the selected zone in (a); (d) EDS of the selected zone in (b).

Table 1
Parameters of plasma spraying.

Parameters	VPS bond coat	APS top coat
Gas Ar (slpm)	50	35
Gas H_2 (slpm)	9	9
Current (A)	720	550
Voltages (V)	64	66
Spray distance (mm)	275	90
Powder feeding rate (g/min)	43	22
Surrounding atmosphere pressure (Pa)	1×10^4	$\sim 10^5$

Table 2
Parameters of PVD Al_2O_3 film.

Parameters	Values
Vacuum degree (Pa)	5×10^{-3}
Substrate bias (V)	−100
Discharge current (A)	50
Time (min)	60

Thermal cycle tests of the samples were performed using a tube furnace. The heating time was 30 min at 1100 °C, and then the heated samples were moved into water and dried by compressed air. The microstructure and chemical composition of the coatings were examined by scanning electron microscopy (SEM, JXA-8100, JEOL Japan) equipped with energy dispersive spectrometer (EDS, INCA ENERGY, UK).

The residual stresses of the coatings were analyzed using micro-Raman spectroscopy (LabRam-1B, Dilor, France). Determination of the residual stresses by Raman spectroscopy is based on peak shifts of Raman bands due to stresses and conversion of these shifts into stress values by the use of tensor coefficients known as phonon deformation potentials or piezo-spectroscopic coefficients. In polycrystalline materials, the average stress tensor $\langle\sigma\rangle$ is related to the shift $\Delta\Omega$ of a given Raman line by

$$\langle\sigma\rangle = -b\Delta\Omega \quad (1)$$

where $\Delta\Omega = \Omega - \Omega_0$ and Ω_0 is the position of selected Raman line for stress-free sample. In other words, a linear relationship between the applied average stress and the peak shift $\Delta\Omega$ is expected. In the present study, the strong Raman line with $\Omega_0 = 470\ \mathrm{cm}^{-1}$ was used for the determination of the residual stresses and the variation of $\Delta\Omega$ at $470\ \mathrm{cm}^{-1}$ was used to represent the variation of residual stress in the TBCs.

3. Results and discussion

3.1. Microstructure of bond coat and TBCs

Fig. 1 shows the surface morphologies of the CoNiCrAlY bond coat with and without PVD Al_2O_3 film. As shown in

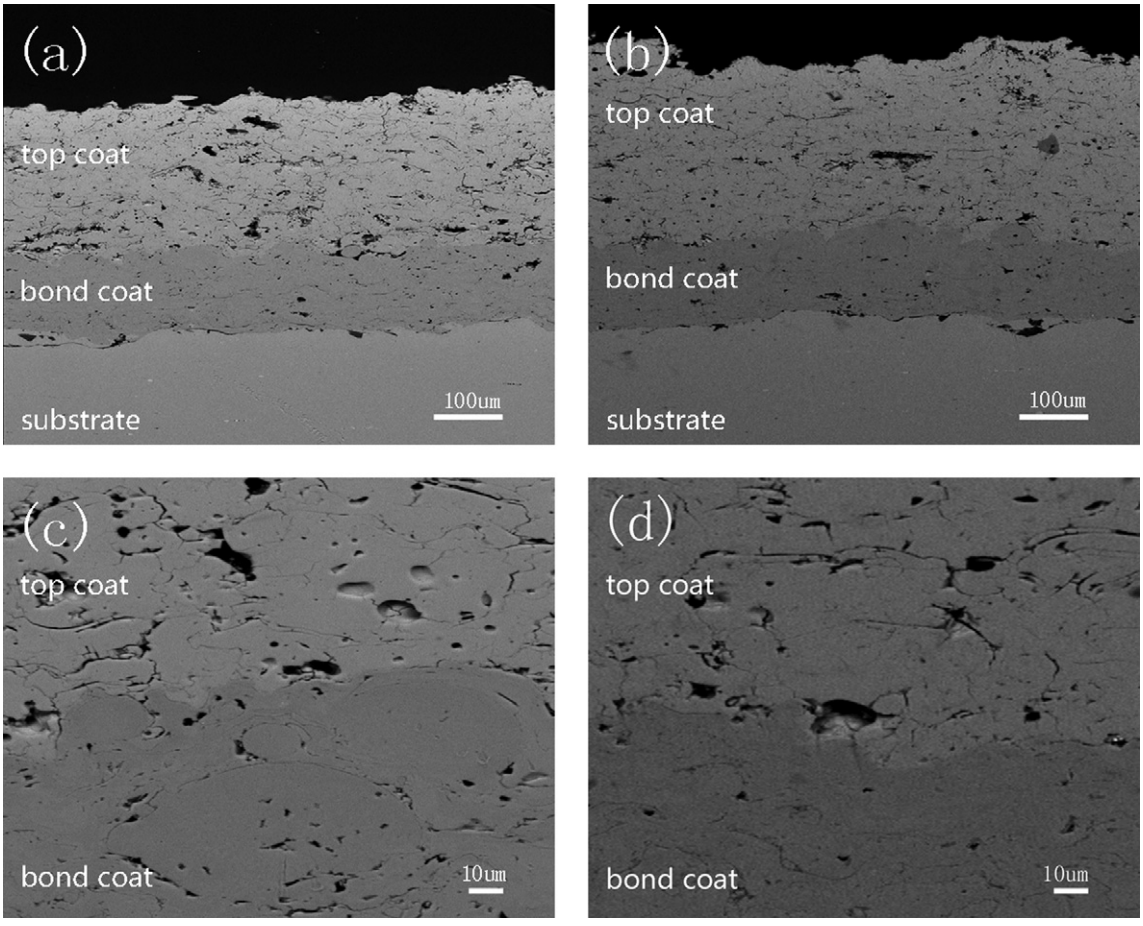

Fig. 2. Cross-sectional SEM images of the as-sprayed TBC systems: (a), (c) conventional; (b), (d) with PVD Al_2O_3 film.

Fig. 1a, the CoNiCrAlY bond coat presented a rough and uneven surface, which was composed of well-flattened splats and partially-molten particles. After the deposition of Al_2O_3 film, no significant change was observed for the surface morphology of the bond coat (Fig. 1b).

The EDS analysis (Fig. 1c and d) shows that the average concentration of aluminum element on the surface of the bond coat had an obvious increase after the deposition of Al_2O_3 film. Elements of Cr, Co and Ni were also detected on both of the two coatings. Although the Al_2O_3 film was too thin to prevent the EDS from detection of the elements beneath it, a reinforcement of Al element could be obviously viewed from the results.

The cross-section micrographs of the YSZ/CoNiCrAlY TBCs are shown in Fig. 2. As seen from Fig. 2a and c, the coating showed lamellar structure which was the characteristics of plasma spraying deposition [4]. A relatively high porosity could be observed for the YSZ top coat, which was considered to be helpful to the thermal insulation ability of the coating. The bond coat exhibited a denser microstructure that could ensure good protection of the substrate against thermal oxidation and

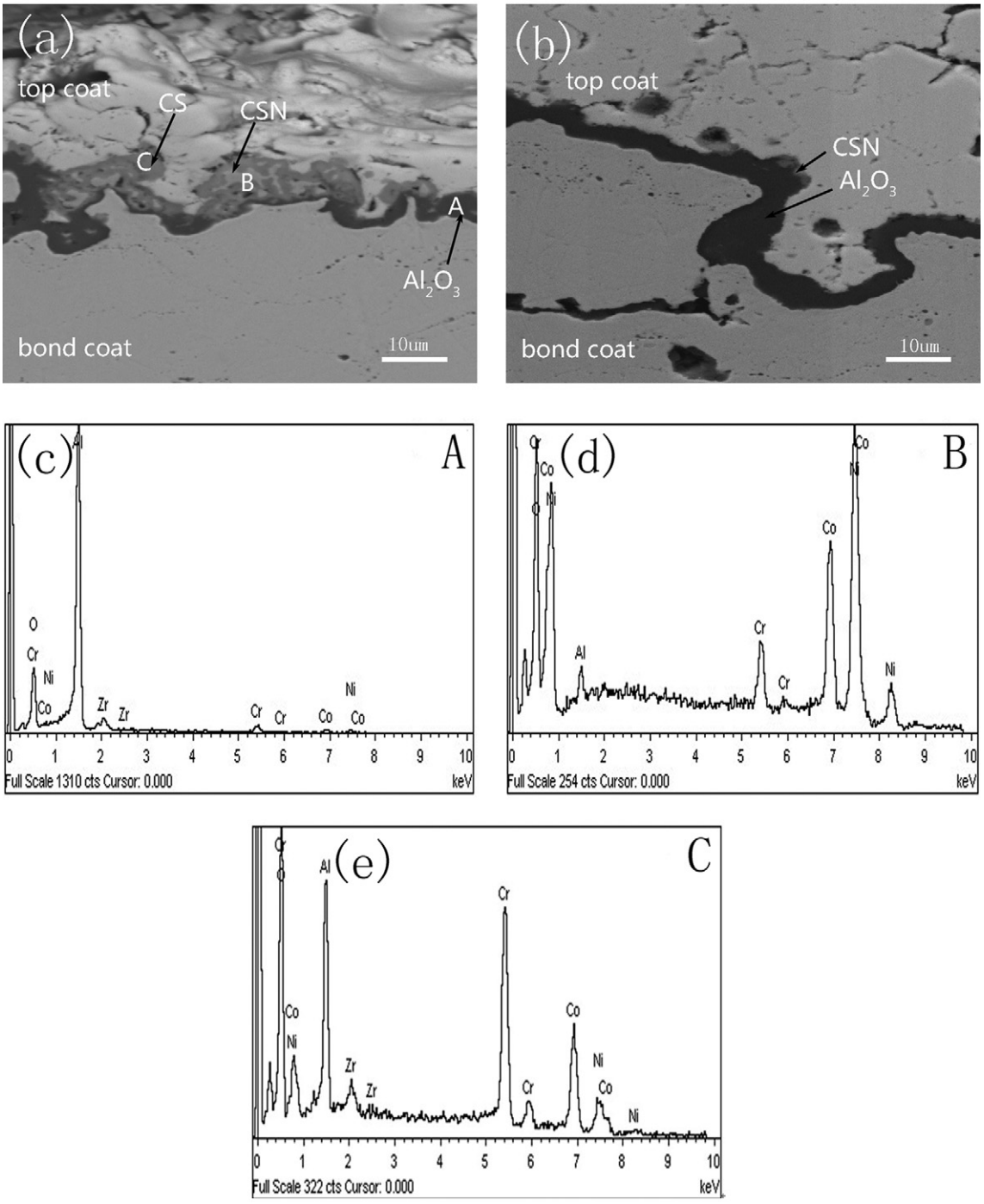

Fig. 3. Cross-sectional SEM images and energy dispersive spectra (EDS) of TBC systems after 40 cycles: (a) cross-sectional image of conventional TBC system; (b) cross-sectional image of modified TBC system; (c) EDS analysis at point A; (d) EDS analysis at point B; (e) EDS analysis at point C.

corrosion. It also could be seen from Fig. 2a and c that the ceramic top coat, bond coat and substrates were well connected and the oxidation phenomenon was not noticeable. After the deposition of PVD Al_2O_3 film in the TBC system, no additional change of the coating microstructure could be observed (Fig. 2b and d) since the film was too thin.

3.2. TGO layer growth

Microstructures and chemical compositions of the TGO layer in the YSZ/CoNiCrAlY TBC after 40 thermal cycles, are presented in Fig. 3. After high temperature service, TGO layer developed at the interface of the top and bond coats in the both TBC systems (as shown in Fig. 3a and b). In the TGO layer of the conventional TBC system, besides Al_2O_3, mixed oxide clusters appeared abundantly, which were comprised of $(Cr,Al)_2O_3 + (Co,Ni)(Cr,Al)_2O_4 + NiO$ (CSN), and $(Cr,Al)_2O_3 + (Co,Ni)(Cr,Al)_2O_4$ (CS) [5]. The existence of CSN and CS in TGO layer is normally considered as a weakness for TBCs [6]. The TGO layer was found more uniform and compact in the modified TBC system as compared with the conventional one. No CS cluster was found and the formation of CSN was also significantly limited (Fig. 3b).

In the conventional TBC system, the concentration of oxygen at the ceramic/bond coat interface was relatively higher than the critical concentrations for the formation of all oxides of metals which constituted the bond coat, owing to the inherent porosity of the top coat and the high oxygen permeability of YSZ [12]. Nonselective oxidation happened, and alumina, CSN and CS formed at the ceramic/bond coat interface. As for the TBC system with PVD Al_2O_3 film, the diffusion of oxygen from the top coat to the bond coat was retarded, and the concentration of oxygen at the ceramic/bond coat interface became lower. Preferential oxidation of Al took place, and the formation of CSN and CS clusters was limited.

Cross-sectional SEM images of TBCs after 137 thermal cycles are shown in Fig. 4. The TGO layer in the conventional TBC system obviously became dispersive, and some voids appeared in the bond coat along the border of ceramic/bond coat interface, most of which collected at the regions connected to CSN clusters, as shown in Fig. 4a. This made these regions porous and decreased the resistant to crack propagation [5]. Some cracks paralleled to the TGO layer were found in the top coat, which were also mostly associated with the CSN clusters. While in the modified TBC system, a rather uniform and compact TGO layer of predominantly Al_2O_3 was formed at the ceramic/bond coat interface (Fig. 4b).

3.3. Element distribution in and near TGO layer

Figs. 5 and 6 exhibit the cross-sectional line scans for the conventional TBC system before and after 137 thermal cycles. The element of Al was mainly in the bond coat, while Zr, O and Y were distinguished for the top coat, as indicated in Fig. 5. After thermal cycles there were no substantial changes for the Zr and Y elements, whereas the concentrations of O and Al increased remarkably at the interface of bond coat/YSZ, which revealed the presence of Al_2O_3 (Fig. 6). The shape of O spectrum was nearly symmetrical (Fig. 6c), while Al exhibited an asymmetrical spectrum where the intensity of the peak along the bond coat side was obviously higher (Fig. 6b). It implied that the higher peaks of Al arose from Al_2O_3 and the zone corresponding to lower peaks was occupied by the other mixed oxides, such as CSN and CS. In addition, the amount of Al decreased in the internal zone of the bond coat which indicated the Al-depletion phenomenon [18].

The cross-sectional line scan for the modified TBC system after 137 thermal cycles in Fig. 7 shows that both of the Al and O rich areas were symmetrical and with almost same peak width. It implied that the oxides at the interface of bond/YSZ were primary Al_2O_3, while the formations of CSN and CS were mostly retarded. The rich areas of Al and O (Fig. 7b and c) were much narrower than those for the conventional TBC system, which meant the thickness of the TGO layer in the Al_2O_3/YSZ system was much thinner than that on the conventional one, suggesting that the growth of TGO layer was obviously restricted by the pre-deposition of PVD Al_2O_3 film.

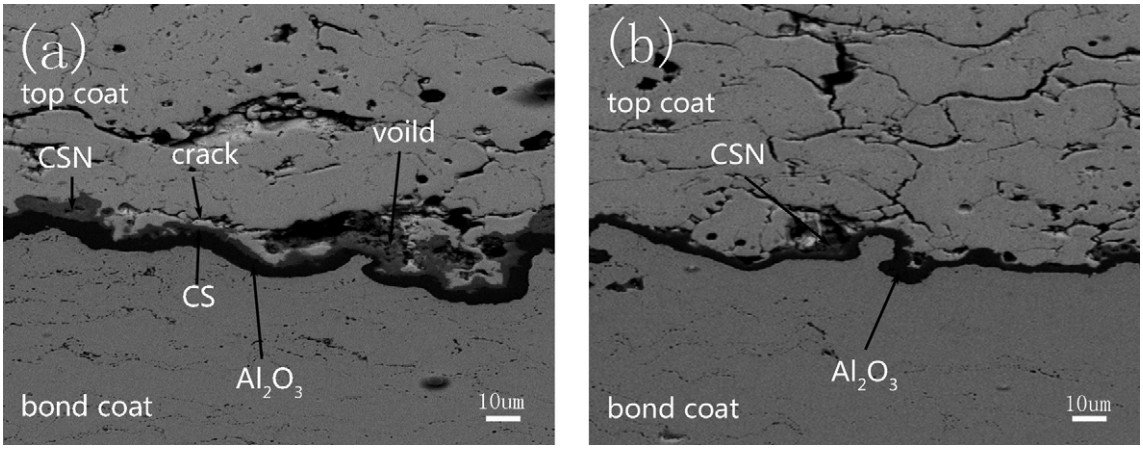

Fig. 4. Cross-sectional SEM images of TBC systems after 137 cycles: (a) cross-sectional image of conventional TBC system; (b) cross-sectional image of modified TBC system.

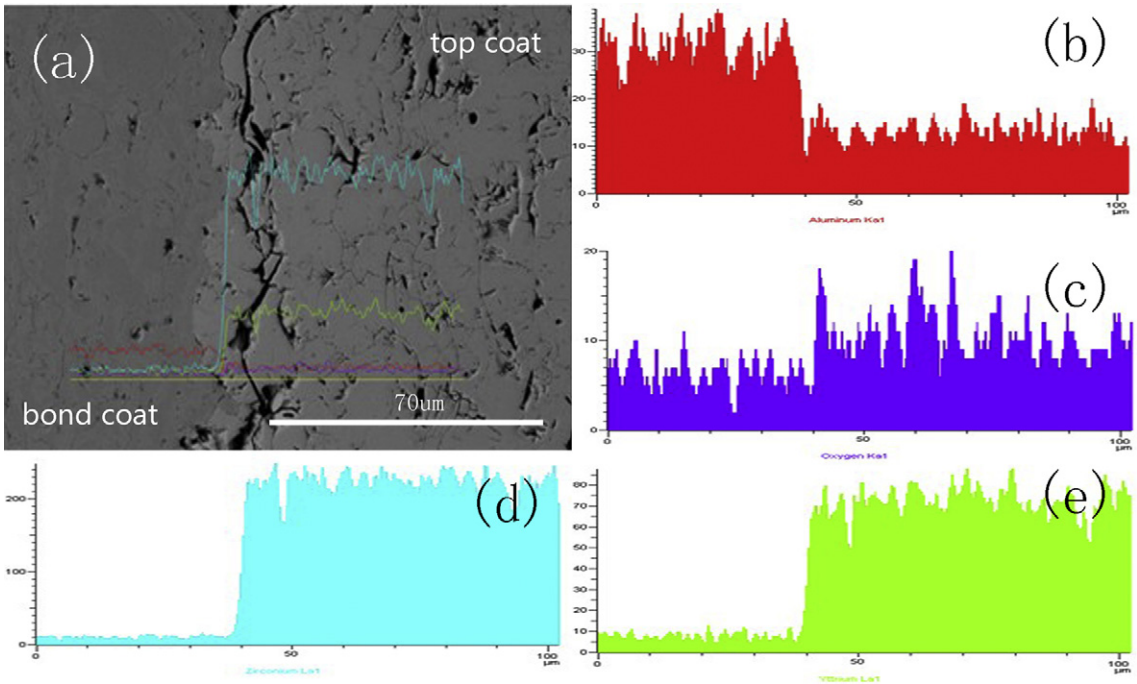

Fig. 5. Cross-sectional line scan images of the conventional TBC system: (a) SEM image; (b) Al; (c) O; (d) Zr; (e) Y line scans of (a).

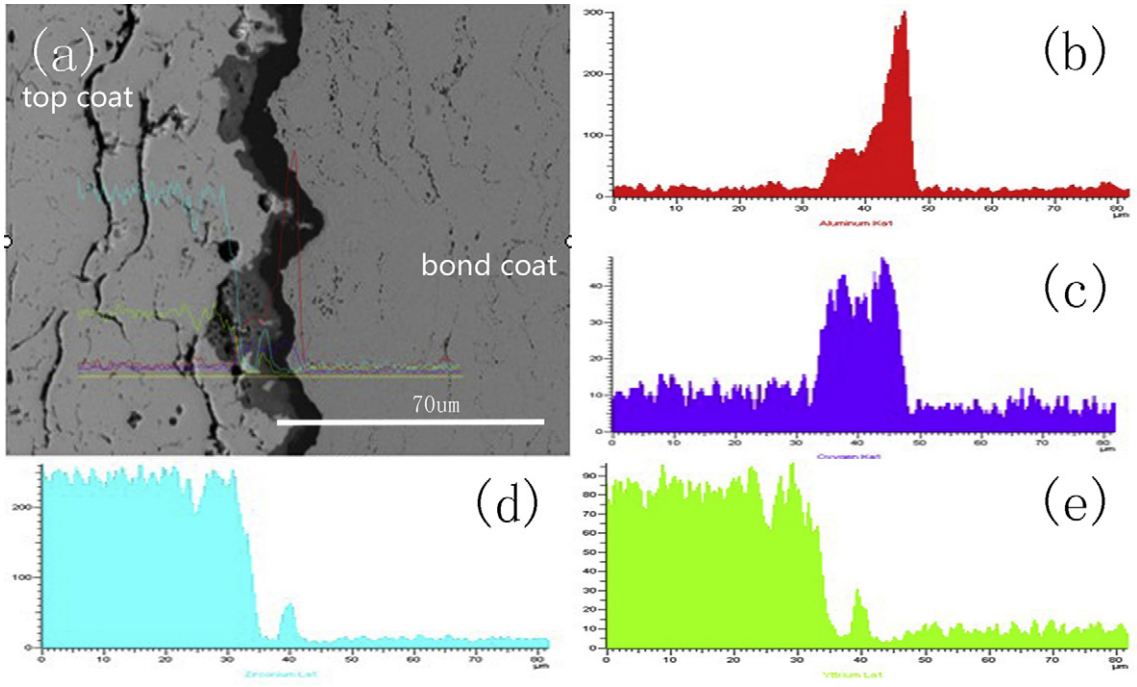

Fig. 6. Cross-sectional line scan images of the conventional TBC system after 137 thermal cycles: (a) SEM image; (b) Al; (c) O; (d) Zr; (e) Y line scans of (a).

3.4. Residual stresses in top coat

Figs. 8 and 9 show the Raman spectra obtained for YSZ top coat in the conventional and modified TBC systems before and after thermal cycles. Similar peaks (the meanings were listed in Table 3 [13,19,20]) appeared in both of the spectra for the conventional and modified TBC systems. Tetragonal phase was found for the zirconia, while no evidence of monoclinic phase was observed. After thermal cycles, the profile between 550 and 700 cm^{-1} decomposed to 620 and 640 cm^{-1} (Fig. 8b). The band at 260 cm^{-1} became narrower after thermal cyclic testing, which suggested that the oxygen vacancies decreased and the compress stress in the coatings increased [21,22].

The spectral shifts $\Delta\Omega$ (the band at 470 cm^{-1}) in the conventional and modified TBC systems are shown in Table 4. From the change of $\Delta\Omega$, the variation trend of residual stresses could be studied. It could be viewed that tensile stresses were presented in the samples without thermal oxidation and

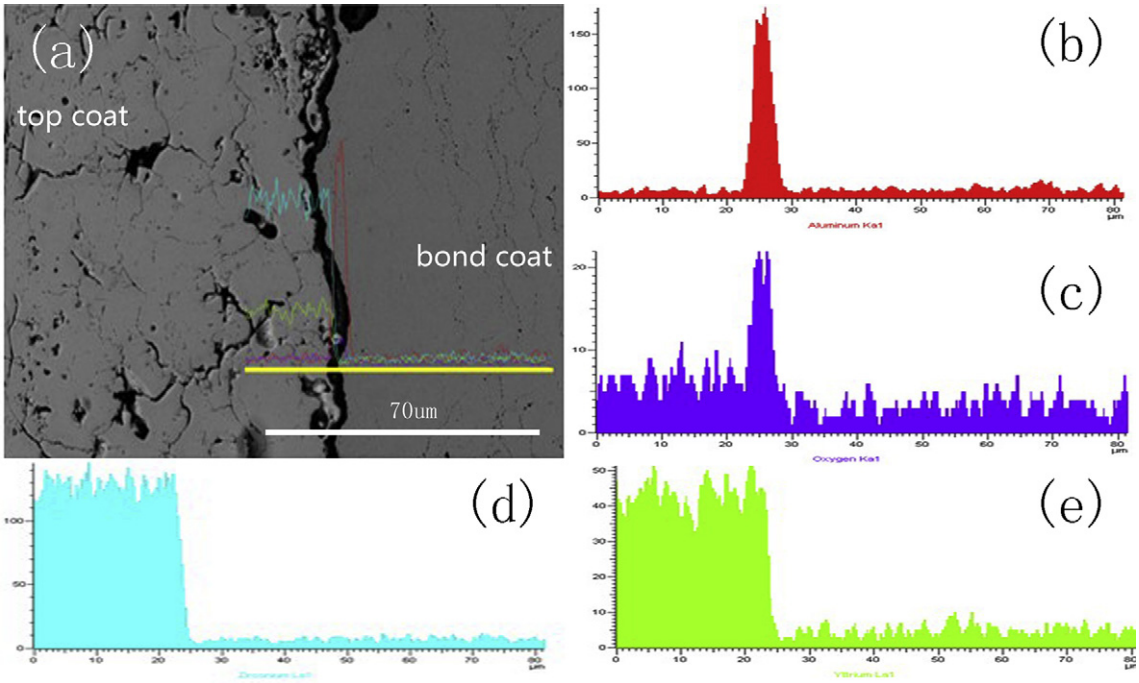

Fig. 7. Cross-sectional line scan images of the modified TBC system after 137 thermal cycles: (a) SEM image; (b) Al; (c) O; (d) Zr; (e) Y line scans of (a).

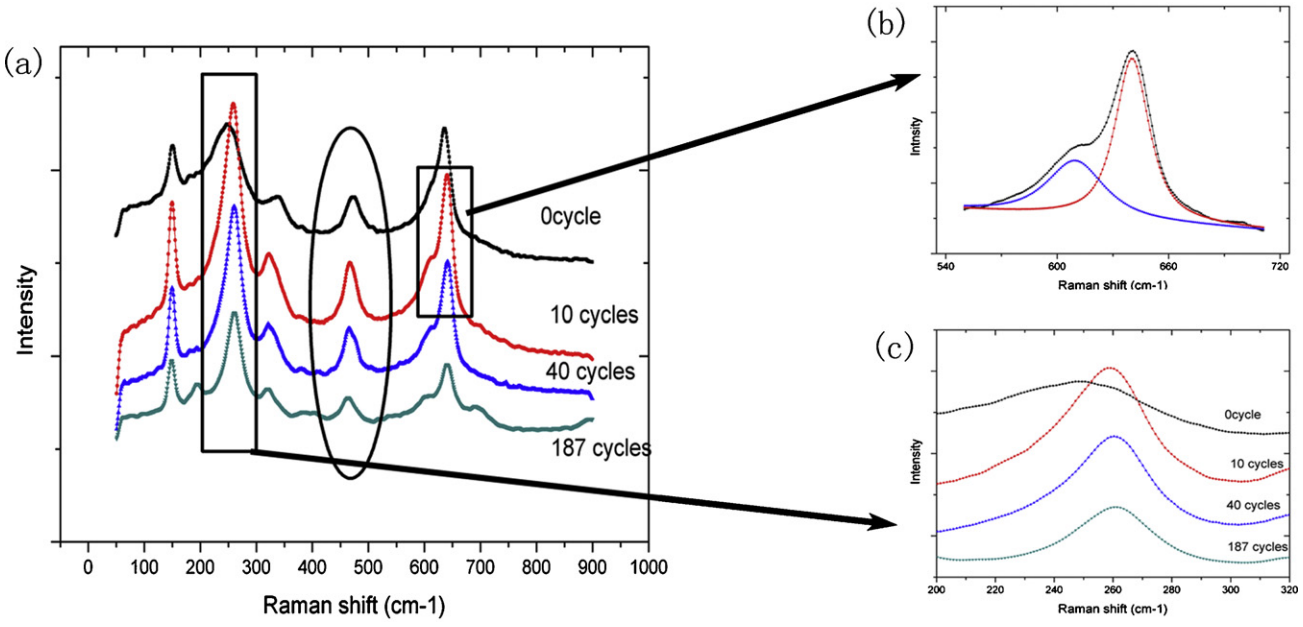

Fig. 8. Raman spectra of the conventional TBC system after different thermal cycles.

transformed into compressive residual stresses after 10 cycles of thermal shock testing. With the increasing of thermal cycles, the compressive residual stresses increased. It also could be distinguished that the residual stresses in conventional top coat were obviously larger than that in the modified TBC system. TGO layer usually possesses large residual compressive stresses when it cools down to ambient temperature, because of its thermal expansion mismatch with substrate [8]. During the follow-up thermal cycles, stress relieving occurs and usually accompanies with tensile stresses parallel to TGO/ceramic layer interface that could lead to crack and spallation at the interface. It is obvious that thicker TGO layer induces higher residual stresses in top coat [4]. The formation of uniform and compact TGO layer (Fig. 4) in the modified TBC system was helpful to mitigate the residual stress in the YSZ coat.

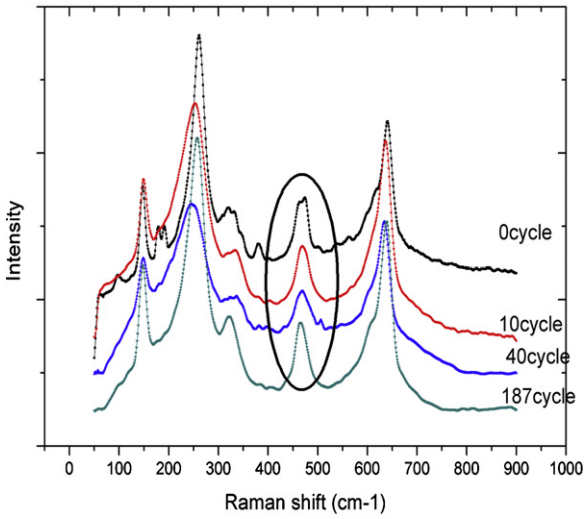

Fig. 9. Raman spectra of modified TBC system after different thermal cycles.

Table 3
Wave numbers, symmetries, structural phase assignments and vibration band of YSZ.

Wave number (cm^{-1})	Symmetry	Phase assignment	Vibration band
148	B_1g	T	O_I–Zr–O_I and Zr–O_I–Zr
258	A_1g	T	Zr–O_{II}
318	B_1g	T	O_I (or O_{II})–Zr–O_I (or O_{II})
470	Eg	T	O_I (or O_{II})–Zr–O_I (or O_{II})
610	B_1g	T	Zr–O_I
641	Eg	T	Zr–O_I

Table 4
Spectral shift $\Delta\Omega$ of the band at 470 cm^{-1} in the YSZ top coat.

Cycles	$\Delta\Omega$ (cm^{-1}) in conventional TBC system	$\Delta\Omega$ (cm^{-1}) in modified TBC system
0	2.83	2.04
10	−2.43	−0.20
40	−2.57	−2.22
137	−5.67	−4.95

4. Conclusions

A novel thermal barrier coating (TBC) system with pre-deposition of Al_2O_3 film on CoNiCrAlY bond coat was developed. It was found that the morphology, thickness and composition of thermally grown oxide (TGO) layer formed after high temperature service were apparently changed. The TGO layer became denser and more consecutive than that in the conventional TBC. The phase composition of TGO was predominantly Al_2O_3, and some other mixed oxide clusters like chromia, spinel, and nickel oxide (CSN), which existed largely in the conventional system, were obviously limited in the modified system. We attributed these changes to the oxygen diffusion retarding effects by the dense pre-deposited Al_2O_3 film. The compressive residual stresses were also reduced in the modified TBC system under working condition due to these changes and confinement of the TGO layer.

References

[1] W.R. Chen, X. Wu, B.R. Marple, P.C. Patnaik, Oxidation and crack nucleation/growth in an air-plasma-sprayed thermal barrier coating with NiCrAlY bond coat, Surface & Coatings Technology 197 (2005) 109–115.
[2] G.W. Goward, Progress in coatings for gas turbine airfoils, Surface & Coatings Technology 108 (1998) 73–79.
[3] A.C. Karaoglanli, E. Altuncu, I. Ozdenir, A. Turk, F. Ustel, Structure and durability evaluation of YSZ + $Al_{(2)}O_{(3)}$ composite TBCs with APS and HVOF bond coats under thermal cycling conditions, Surface & Coatings Technology 205 (2011) S369–S373.
[4] A. Kobayashi, M. Saremi, A. Afrasiabi, Microstructural analysis of YSZ and YSZ/Al_2O_3 plasma sprayed thermal barrier coatings after high temperature oxidation, Surface & Coatings Technology 202 (2008) 3233–3238.
[5] W.R. Chen, X. Wu, B.R. Marple, D.R. Nagy, P.C. Patnaik, TGO growth behaviour in TBCs with APS and HVOF bond coats, Surface & Coatings Technology 202 (2008) 2677–2683.
[6] W.R. Chen, R. Archer, X. Huang, B.R. Marple, T.G.O Growth, Crack propagation in a thermal barrier coating, Journal of Thermal Spray Technology 17 (2008) 858–864.
[7] W.G. Sloof, T.J. Nijdam, Effect of Y distribution on the oxidation kinetics of NiCoCrAlY bond coat alloys, Oxidation of Metals 69 (2008) 1–12.
[8] A.G. Evans, D.R. Mumm, J.W. Hutchinson, G.H. Meier, F.S. Pettit, Mechanisms controlling the durability of thermal barrier coatings, Progress in Materials Science 46 (2001) 505–553.
[9] I.T. Spitsberg, D.R. Mumm, A.G. Evans, On the failure mechanisms of thermal barrier coatings with diffusion aluminide bond coatings, Materials Science and Engineering A-Structural Materials Properties Microstructure and Processing 394 (2005) 176–191.
[10] V.K. Tolpygo, D.R. Clarke, Oxidation-induced failure of EB-PVD thermal barrier coatings, Surface & Coatings Technology 146 (2001) 124–131.
[11] T.J. Nijdam, G.H. Marijnissen, E. Vergeldt, W.G. Sloof, A.B. Kloosterman, Development of a pre-oxidation treatment to improve the adhesion between thermal barrier coatings and NiCoCrAlY bond coatings, Oxidation of Metals 66 (2006) 269–294.
[12] R.D. Jackson, M.P. Taylor, H.E. Evans, X.H. Li, Oxidation study of an EB-PVD MCrAlY thermal barrier coating system, Oxidation of Metals 76 (2011).
[13] A. Scrivani, G. Rizzi, U. Bardi, C. Giolli, M.M. Miranda, S. Ciattini, A. Fossati, F. Borgioli, Thermal fatigue behavior of thick and porous thermal barrier coatings systems, Journal of Thermal Spray Technology 16 (2007) 816–821.
[14] K.J. Kang, S.K. Sharma, G.D. Ko, High temperature creep and tensile properties of alumina formed on Fecralloy foils doped with yttrium, Journal of the European Ceramic Society 29 (2009) 355–362.
[15] H.B. Xu, H.B. Guo, X.F. Bi, S.K. Gong, Preparation of Al_2O_3-YSZ composite coating by EB-PVD, Materials Science and Engineering A-Structural Materials Properties Microstructure and Processing 325 (2002) 389–393.
[16] C.G. Zhou, Q.H. Yu, H.Y. Zhang, F. Zhao, Thermal stability of nanostructured 13 wt% $Al_{(2)}O_{(3)}$-8 wt% $Y_{(2)}O_{(3)}$-$ZrO_{(2)}$ thermal barrier coatings, Journal of the European Ceramic Society 30 (2010) 889–897.
[17] A. Kobayashi, A. Afrasiabi, M. Saremi, A comparative study on hot corrosion resistance of three types of thermal barrier coatings: YSZ, YSZ + Al_2O_3 and YSZ/Al_2O_3, Materials Science and Engineering A-Structural Materials Properties Microstructure and Processing 478 (2008) 264–269.
[18] M. Matsumoto, K. Hayakawa, S. Kitaoka, H. Matsubara, H. Takayama, Y. Kagiya, Y. Sugita, The effect of preoxidation atmosphere on oxidation behavior and thermal cycle life of thermal barrier coatings, Materials

Science and Engineering A-Structural Materials Properties Microstructure and Processing 441 (2006) 119–125.

[19] T. Merle, R. Guinebretiere, A. Mirgorodsky, P. Quintard, Polarized Raman spectra of tetragonal pure ZrO_2 measured on epitaxial films, Physical Review B 65 (2002) 1–6.

[20] F. Capel, M.A. Banares, C. Moure, P. Duran, The solid solubility limit of TiO_2 in 3Y-TZP studied by Raman spectroscopy, Materials Letters 38 (1999) 331–335.

[21] S. Boullosa-Eiras, E. Vanhaecke, T.J. Zhao, D. Chen, A. Holmen, Raman spectroscopy and X-ray diffraction study of the phase transformation of $ZrO_{(2)}$–$Al_{(2)}O_{(3)}$ and $CeO_{(2)}$–$Al_{(2)}O_{(3)}$ nanocomposites, Catalysis Today 166 (2011) 10–17.

[22] S. Nazarpour, C. Lopez-Gandara, F.M. Ramos, Phase transformation studies on YSZ doped with alumina. Part 1: metastable phases, Journal of Alloys and Compounds 505 (2010) 527–533.